PROCEEDINGS OF SPIE

SPIEDigitalLibrary.org/conference-proceedings-of-spie

Early detection of at-risk keratoplasties and prediction of future corneal graft rejection from pre-diagnosis endothelial cell images

Joseph, Naomi, Benetz, Beth Ann, Menegay, Harry, Oellerich, Silke, Baydoun, Lamis, et al.

Naomi M. Joseph, Beth Ann Benetz, Harry Menegay, Silke Oellerich, Lamis Baydoun, Gerrit Melles, Jonathan H. Lass, David Wilson, "Early detection of at-risk keratoplasties and prediction of future corneal graft rejection from pre-diagnosis endothelial cell images," Proc. SPIE 11597, Medical Imaging 2021: Computer-Aided Diagnosis, 115972C (18 February 2021); doi: 10.1117/12.2582171

SPIE.

Event: SPIE Medical Imaging, 2021, Online Only

Early detection of at-risk keratoplasties and prediction of future corneal graft rejection from pre-diagnosis endothelial cell images

Naomi M. Joseph,[a] Beth Ann Benetz,[c,d] Harry Menegay,[d] Silke Oellerich,[e] Lamis Baydoun,[e,f,g] Gerrit Melles,[e,h] Jonathan H. Lass,[c,d] and David Wilson [a,b,*]

[a]Department of Biomedical Engineering, Case Western Reserve University, 10900 Euclid Avenue, Cleveland, OH 44106, USA
[b]Department of Radiology, Case Western Reserve University, 10900 Euclid Avenue, Cleveland, OH 44106, USA
[c]Department of Ophthalmology and Visual Sciences, Case Western Reserve University, 10900 Euclid Avenue, Cleveland, OH 44106, USA
[d]Cornea Image Analysis Reading Center, 6700 Euclid Avenue, Cleveland, OH 44103, USA
[e]Netherlands Institute for Innovative Ocular Surgery (NIIOS), Laan op Zuid 88 – 3071 AA Rotterdam, The Netherlands
[f]University Eye Hospital Munster, Germany
[g]ELZA Institute Dietikon/Zurich, Switzerland
[h]NIIOS-USA, San Diego, USA

ABSTRACT

The status of the donor tissue post-keratoplasty (post-transplant), whether full or partial thickness, is currently assessed for health, function, and complications via clinical evaluations. This includes detection of visible signs of graft rejection on slit lamp biomicroscopy such as keratic precipitates or edema. Corneal endothelial cell (EC) images are utilized to indirectly assess the health of the cornea post keratoplasty with evidence that morphometric changes may occur prior to clinical signs of rejection. We extracted over 190 novel quantitative features from EC images acquired 1-12 months prior to patients´ rejection diagnosis date, and used random forest (RF) classifiers to predict future rejection. We automatically segmented the cell borders of 171 EC images using a semi-automated segmentation approach: deep learning U-Net segmentation followed by guided manual correction. Following segmentation, we extracted novel quantitative features that robustly represented the cellular morphology from the EC images. We trained and tested a RF classifier using 5-fold cross validation and minimal Redundancy Maximal Relevance (mRMR) feature selection. From the 5-fold cross validation, we report an area under the receiver operating characteristic curve (AUC) of 0.87 ± 0.03, a sensitivity of 0.86 ± 0.12, and a specificity of 0.86 ± 0.10. The results suggest we can accurately predict a patient's future graft rejection 1-12 months prior to diagnosis, enabling clinicians to intervene modifying and/or instituting topical corticosteroid therapy earlier with the possibility of lowering graft rejection failures. Success of this classifier could reduce health care costs, patient discomfort, vision loss and the need for repeat keratoplasty.

Keywords: Cornea, machine learning, feature extraction, image processing

1. INTRODUCTION

A healthy endothelial cell (EC) layer maintains a clear cornea by utilizing active ion-pumps to keep the corneal stroma relatively dehydrated by redistributing fluid from the cornea to the anterior chamber. These healthy cells are usually hexagonally shaped, with similar size, and are uniformly aligned. Over time, however, corneal ECs start to die but are never replaced by dividing cells. Instead, surrounding ECs enlarge and undergo a shape change with fewer hexagonal cells. These changes indicate that the endothelial cells are under stress and could ultimately lead to failure of their pump and barrier functions, leading to swelling of the stroma, loss of clarity and eventual deteriorating vision.[1,2] Treatment options include topical hypertonic saline, topical corticosteroids, if there is a reversible inflammatory component, but ultimately require a keratoplasty, one of the most common transplants performed with over 44,000 surgeries annually in the United States.[3] There are three types of keratoplasty procedures available: penetrating keratoplasty (PK), Descemet stripping automated endothelial keratoplasty (DSAEK), and Descemet membrane endothelial keratoplasty (DMEK). Each transplant varies based on how much of the donor's cornea is extracted and implanted into the recipient's eye.[4]

Post-keratoplasty visits are routinely performed to evaluate transplant health and detection of any complications including graft rejection. It is important to note that the current approaches to identify at-risk keratoplasty eyes are

Medical Imaging 2021: Computer-Aided Diagnosis, edited by Maciej A. Mazurowski, Karen Drukker, Proc. of SPIE Vol. 11597, 115972C · © 2021 SPIE
CCC code: 1605-7422/21/$21 · doi: 10.1117/12.2582171

conducted via clinical qualitative evaluations. However, the rejection process can remain asymptomatic, showing no clinical signs in the early stages, making it difficult to identify and reverse before its severity causes more permanent damage to the graft. If during an examination of the cornea via slit-lamp, clinical signs such as keratic precipitates, a rejection line, epithelial and/or stromal edema, or cloudiness of the cornea are evident, this indicates the rejection process has been damaging the endothelium, which could ultimately lead to graft failure, i.e., corneal swelling that deteriorates vision. From here, it would be necessary for a patient to undergo a re-graft, which can accelerate a patient's risk for another rejection or failure. Ultimately, there is a clinical need to detect graft rejection at an earlier stage, such that clinicians can administer treatment plans promptly, potentially reversing the rejection process, ultimately lowering the keratoplasty re-graft rate.

One-way clinicians examine the endothelium for damage, especially to determine a reduction in EC density (ECD) or morphometric changes, is by evaluating specular microscopic images of this corneal layer. This evaluation involves an automatic segmentation by a specular microscope in a small region of a central endothelial image, followed by the calculation of three quantitative biomarkers: ECD, coefficient of variation (CV), and percent hexagonality (HEX). Briefly, ECD is the number of cells per total sample area of cells in the image, CV is the standard deviation of cell area divided by the mean cell area within the image, and HEX is the percentage of cells that have six sides.[5–7] Clinicians use these traditional morphometrics of the EC layer to evaluate cornea health post-transplantation. Some challenges arise however especially when images are of poor quality, and clinicians note that these morphometrics are limited in telling the full story of the graft's deteriorating condition.[8]

Previous attempts at developing risk prediction scales to identify grafts at-risk for a future adverse event are dependent on clinical factors mentioned previously, and demographic data such as donor/recipient gender, prior ocular surgery, glaucoma history, surgical complications, diabetes, etc.[9–12] Monnereau et al. conducted a qualitative analysis of cell arrangement, size, and shape within the endothelium from EC images collected at standardized time intervals post-DMEK. They showed that these morphological characteristics were significantly different between corneal grafts that eventually rejected and corneal graft that never rejected during the study's duration.[4] O'Brien et al. recently published their efforts of utilizing random survival forests to determine possible predictors of DSAEK failure. They trained their survival forests on 50 baseline donor, recipient, and eye bank variables, and found that intraoperative complications were most predictive of a future graft failure.[13] Large clinical studies such as the Specular Microscopy Ancillary Study (SMAS) and the Cornea Preservation Time Study (CPTS) quantitatively examined thousands of corneal EC images post-keratoplasty. The SMAS found that ECD at 6 months, 1 year and 5 years was strongly predictive with subsequent graft failure. Furthermore, 6-month HEX results suggested an association with subsequent graft failure, whereas CV was not predictive of graft failure.[14,15] The CPTS found that lower ECD at 6-months post-endothelial keratoplasty was associated with future graft failure. It was also reported that experiencing a rejection episode is associated with higher endothelial cell loss at 3-years post-endothelial keratoplasty.[16–18]

These studies show the benefit of analyzing EC images, cell morphology, and utilizing machine learning techniques to identify predictive factors of future adverse events, encouraging us to evaluate keratoplasties more quantitatively from an imaging approach. We propose an image analytics solution, starting with a semi-automatic deep learning approach to segment the dark cell borders of corneal EC images following a keratoplasty. From these segmentations we can extract and utilize an extensive collection of quantitative features to train and test a machine learning classifier to predict future graft rejection.

2. IMAGE PROCESSING AND ANALYSIS

The image analysis portion of our solution involves two steps: automated cell segmentation and cellular/image feature extraction. The automated cell segmentation will utilize convolutional neural network U-Net. This deep learning algorithm will use probabilities to classify all pixels in the image into two categories, namely cell border and other. Probability outputs from the network shows areas of high and low classification confidence. After the segmentations are finalized, we measure and calculate over 190 quantitative features that robustly describe the cells' shape and size within a given image. More details regarding the nature of these features will be discussed in the following sections.

2.1 Semi-automated deep learning segmentation

Our U-Net deep learning segmentation begins with pre-processing the EC images to remove the illumination gradient that exists across the images from left to right. To remove this gradual change from dark to light intensity, we apply a Gaussian

filter with standard deviation $\sigma = 21$ and kernel footprint (65 x 65 pixels) producing a background image. The original EC image is subtracted by this background image, and then the 99th percentile of the image's intensity is set to 255 before normalizing the rest of the image's intensity within the range (0, 255).

After pre-processing the EC images, we use the U-Net neural network architecture proposed by Ronneberger et al. shown in Fig. 1 below, which has shown promising results with regards to image segmentation.[19] U-Net has many advantageous features such as its decoding (downsampling), encoding (upsampling), and skip connections allowing the network to recover full spatial resolution in its decoding layers. The architecture contains 16 layers and has a receptive field of size (68, 68). U-Net produces probability output images with pixel values between 0 and 1. Values closer to 0 indicate strong confidence of a cell's border, and values closer to 1 indicate strong confidence of a cell or other surrounding.

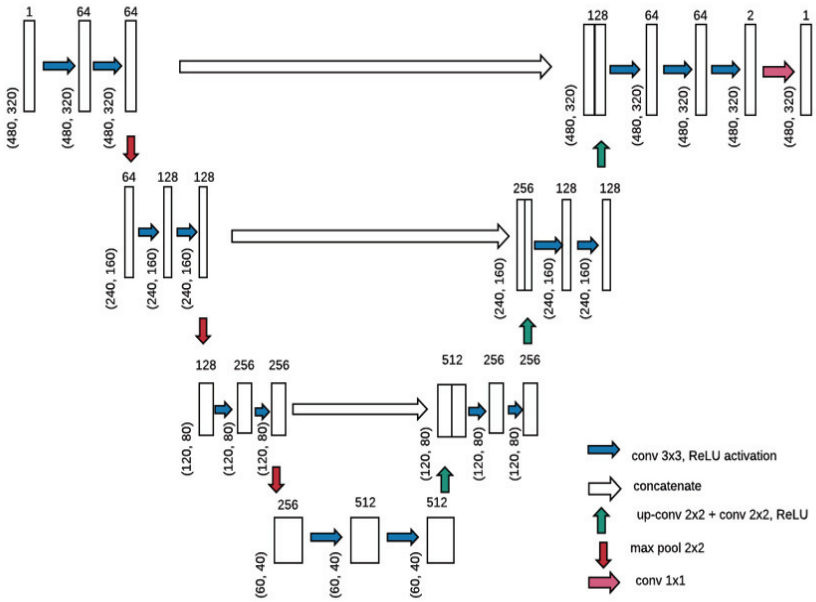

Figure 1. U-Net architecture. The network consists of multiple encoding and decoding steps with three skip connections between the layers (white arrows). Numbers on top and the left bottom corner of each tensor indicate number of channels/filters and its height and width, respectively. Arrows are color-coded as follows: blue: convolution with (3, 3) filter size, rectified linear unit (ReLU) activation, green: up-convolution with a (2, 2) kernel using max pooling indices from the encoding layers, red: max pooling with a (2, 2) kernel, pink: (1, 1) convolution with sigmoid activation.

Following U-Net, the probability output images undergo a post-processing pipeline to binarize and clean up the cell borders until the result is a binary image with single pixel-width black borders that fully enclose white cells. This pipeline starts with first upscaling the probability outputs from values (0 to 1) to create (0 to 255) grayscale images. From here, the grayscale images are binarized using an adaptive Otsu threshold, followed by five morphological operations to create thin borders between cells and to clean the binarized result. The result is a binary image with single-pixel width black borders that is closed and fully encapsulates white cells, with white surrounding area.[20]

We created a Guided Manual Correction graphical user interface (GUI) software to deal with the U-net segmentation errors, whereby an operator can quickly identify suspicious cells for correction. Our GUI software was developed in the Python programming language version 3.7. The software displays the final segmentation border image after post-processing overlaid the corresponding pre-processed EC image, and provides the user with a pen and eraser tool for editing the segmentation image. We have implemented two conditions to identify suspicious cells for editing in each image. We define suspicious cells as over-segmented (when one true cell has been split into two or more cells) or under-segmented (when two or more cells have been merged into one cell).

2.2 Feature Extraction

The second step entails an extensive quantitative analysis by extracting 193 features from the following three broad categories: 1) traditional morphometrics (i.e., ECD and CV); 2) cell-graph analytics (e.g., Voronoi tessellation, Delaunay

triangulation, and cell cluster graph metrics); and 3) traditional cellular architectural morphometrics (e.g., area, shape, intensity, and eccentricity). The latter category of features is measured on a cell-by-cell basis, by isolating each cell in the original EC image based on connected components from the image's corresponding segmentation. Then, the cell features are condensed to a single image representation by computing the mean, standard deviation, kurtosis, and binned histogram values of the collective cell features. A few features will remain global features (i.e. number of cells). Expanding on cell-graph analytics, these first require the construction of such cell graphs. From here, we measure parameters including the perimeters and areas of cell graph regions, chord lengths connecting cell centroids, and the proximity of cell centroids. In this study, we will be comparing our method of image analysis to current qualitative and quantitative methods. These include a subjective grading scale established by the Netherlands Institute for Innovative Ocular Surgery (NIIOS) and solely traditional morphometrics (ECD, CV, and number of cells).

3. EXPERIMENTAL METHODS

3.1 U-Net Training and Testing

Two datasets of corneal EC images were used in this study, one for training and one for testing. The training dataset consisted of 130 images randomly selected from the CPTS, obtained from the Cornea Image Analysis Reading Center (CIARC) along with their corresponding corner analysis performed in HAI CAS/EB Cell Analysis System software (HAI Laboratories, Lexington, MA). The CPTS acquired EC images from 1330 eyes taken at various time points between 6- to 48-months post-DSAEK. All 130 images used were same-sized (446 x 304 pixels) and the pixel area was 0.65 μm^2 and were taken with Konan specular microscopes (Konan Medical, Irvine, California). Each image contained between 8-130 cells that were manually identified and their borders were segmented. The EC densities of these images ranged from 600 to 2450 cells/mm^2. Figure 2 below shows examples of images within the training dataset.

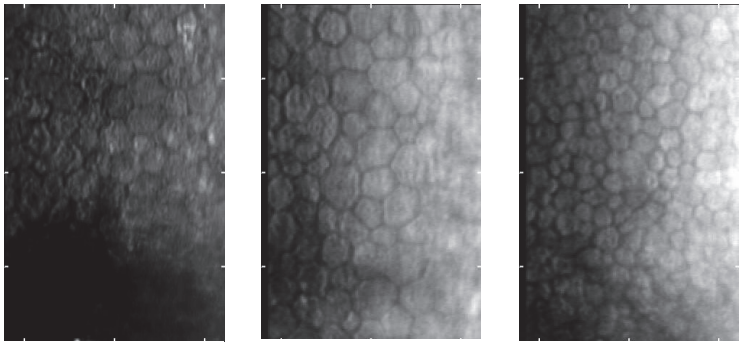

(a) (b) (c)

Figure 2. Three example images of challenging post-DSAEK EC images from the CPTS training dataset with varying ECD.

NIIOS provided the testing dataset of 171 EC images from eyes that had undergone a DMEK. The cohort contained images from both rejection eyes (83 images from 21 eyes) and control eyes with no rejection episodes (88 images from 22 eyes). The rejection images were acquired from each eye at the post-surgery appointment immediately before the rejection diagnosis appointment. Each rejection eye had between 2-4 images taken at this appointment. The control eye images were acquired from up to 3 post-surgery appointments prior to the last appointment for a given patient. All images were deidentified and handled in a method approved by the University Hospitals Cleveland Medical Center Institutional Review Board. Figure 3 below shows examples images from the testing dataset.

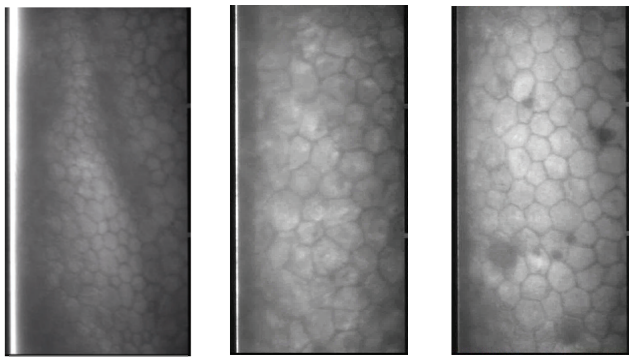

(a) (b) (c)

Figure 3. Three example images of challenging post-DMEK EC images from the NIIOS testing dataset with varying ECD.

Prior to the training process, both training and testing EC images were resized appropriately so that each pixel represented 0.8 μm^2 in area. Following resizing, the images were preprocessed (as described previously) and then padded on all sides in a symmetric fashion to ensure the convolutions are valid at the edges. U-Net was trained on the CPTS dataset of 130 EC images, for a maximum of 200 epochs, using weighted binary cross entropy as its loss function. Class imbalance could be accounted for by weighting the loss function by the inverse of the observed class proportions. For example, in our study, cell borders occurred at a low frequency across all EC images (about 5% of the pixels) whereas cells or other accounted from about 95% of the pixels. Therefore, cell border pixels will have a larger weight in the computation of the lass function. The network was optimized using the Adam optimizer with an initial learning rate of 1.0e-4. Finally, we utilized data augmentation to ensure good generalization performance by the network. Briefly, the augmentations used were in the range of 5% translations in height and width across the image, 5% zoom, 3 deg shear, and random horizontal flips. The trained network was then applied and tested on the NIIOS dataset of 171 images.

Software for image preprocessing and binarizing the network predictions were implemented using MATLAB R2018a. U-Net was implemented using the Keras API (with Tensorflow as backend), the Python programming language. Neural network training was performed using two NVIDIA Tesla P100 graphics processing unit cards with 11 GB RAM on each card.

3.2 Random Forest Classifier

We trained three random forest classifiers on three different 'feature types' extracted from the 171 NIIOS images and their derived cell/cell border segmentations. We chose to use random forest models as they performed better than comparable support vector machine (SVM) classifiers. For each experiment we performed 5-fold cross validation, training on features from 80% of the NIIOS images (141 images) and testing on features from the remaining 20% of the dataset (30 images). Between all 5-folds, the images were stratified by patient eye. Hyperparameters included 250 trees, 35 maximum number of splits, and 10 for the minimum leaf size. Metrics such as area under the receiver operating characteristic curve (AUC), accuracy, sensitivity, and specificity were used to evaluate the performance of the classifiers on each fold's test set.

For the first experiment, the classifier was trained on a subjective grading scale established by NIIOS. This scale was defined by cell morphology, cell distribution, and cell activation. Images given a score of 1 consisted of regularly and consistently shaped cells with no cellular activation, while images with a score of 5 were deemed to have irregular cell morphology and distribution along with high cellular activation. For the second experiment, we used traditional morphometric features such as ECD, CV, and the number of cells in a given image to train and validate the model. Finally, for the third experiment, we used minimum redundancy maximum relevance (mRMR) feature selection to identify the top 10 most predictive features from the previously described 193 quantitative features. This final experiment represents our proposed approach to develop a more robust and quantitative approach for accurately distinguishing between rejection and control corneal grafts.

4. RESULTS

We show results of the automatic segmentation algorithm on two held-out test EC images in Fig. 4. Note that the pre-processing algorithm is able to brighten the original image as well as remove the illumination gradient across the EC image (b). Comparing the segmentation result following our post-processing pipeline (d) to the manually edited results (e), only a couple additional borders or erasing of cell borders is necessary to clean up our automatic algorithm output. These few edits we highlight in the red circles, tend to exist in uncertain areas in the probability output images (c) or hard to distinguish regions within the pre-processed images (b).

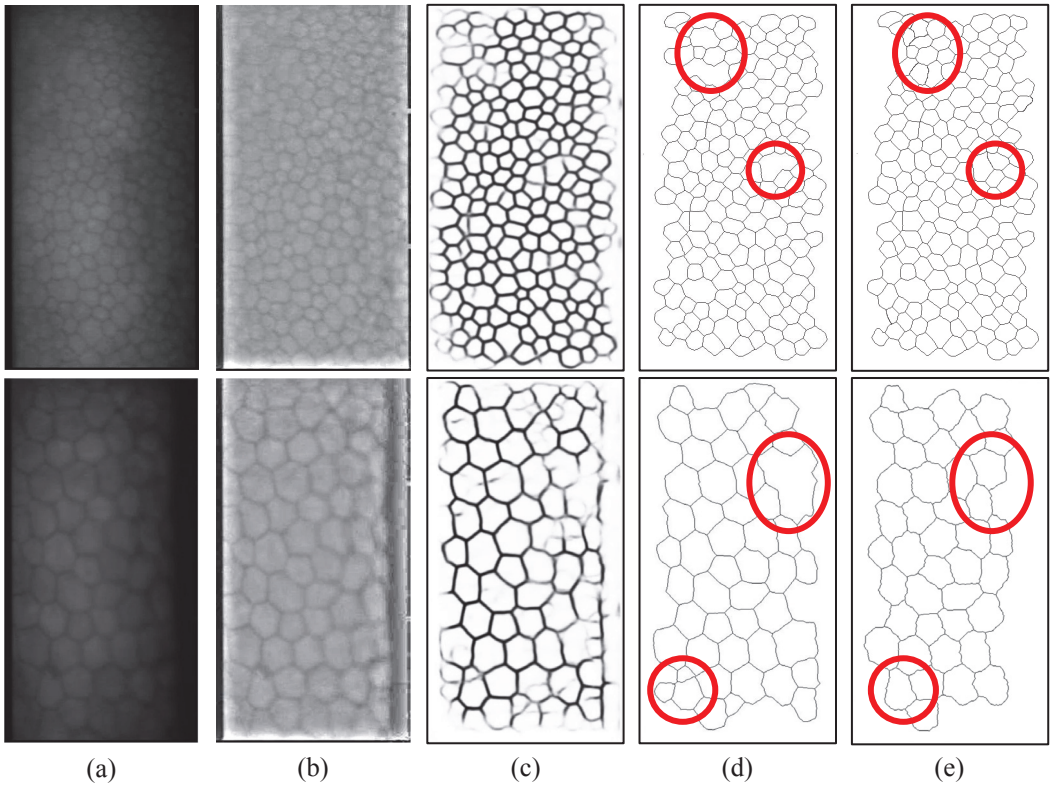

Figure 4. Two example post-DMEK EC images having undergone both manual and automatic segmentation. (a) Original, raw EC images. (b) Enhanced, pre-processed EC images. (c) U-Net probability outputs. (e) Segmentations following post-processing pipeline. (f) Manually edited segmentations using Guided Manual Correction Software. Red circles indicate cells that needed additional edits from (e) to (f).

As mentioned previously, we conducted three experiments, two of which utilized features directly extracted from our semi-automatically generated segmentations and their corresponding EC images. Our proposed approach used mRMR to determine the top ten predictive features, listed in Table 1 below. Of the top 10 predictive features, seven come from graph analytic features, two from shape features, and one from intensity-based features. It is also worth noting that none of the traditional morphometrics (ECD, CV, or number of cells) are deemed most predictive by mRMR.

Table 1. Top 10 Predictive Features Determined by mRMR

Importance Rank	Feature
1	Cluster Cell Graph: Percentage of central nodes
2	Standard Deviation of the number of cell pixels weighted intensities between 205-255
3	% of cells with circularity between 1.04 and 1.3
4	Average distance of cell centroid to 5 Nearest Neighbors
5	Voronoi: Tessellation Perimeter Minimum/Maximum
6	Voronoi: Tessellation Perimeter Standard Deviation
7	Mean Cell Perimeter
8	Delaunay: Triangle Area Minimum/Maximum
9	Voronoi: Tessellation Area Minimum/Maximum
10	Delaunay: Triangle Side Length Average

Below in Figure 5 we show the confusion matrices that illustrate the performance of the three models trained in this study. Our approached proved more accurate, sensitive, and specific in comparison to state-of-the-art approaches (Models 1 and 2), and this is quantitatively demonstrated in Table 2 below as well.

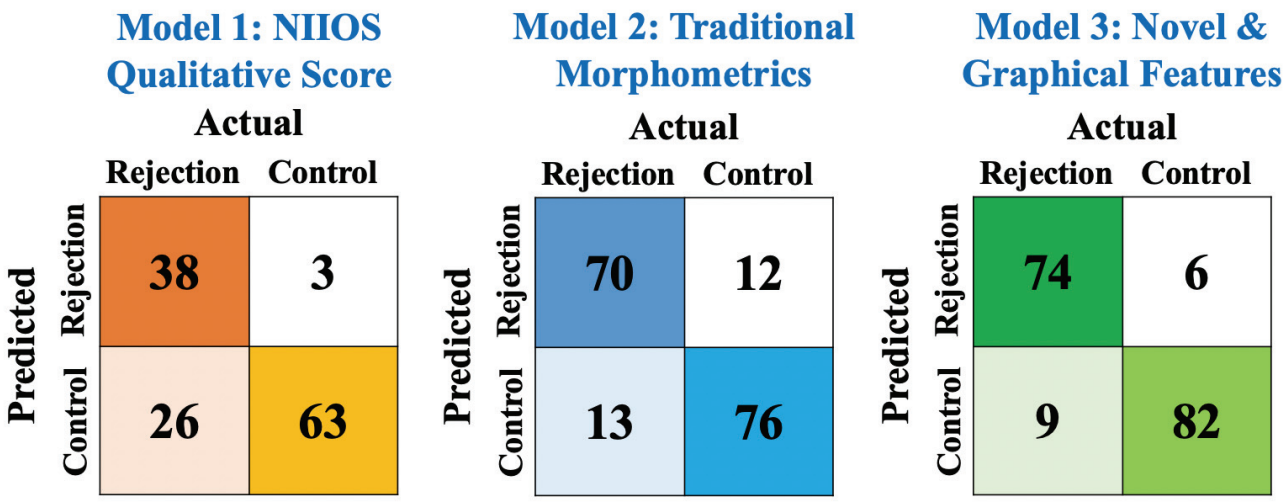

Figure 5. Confusion matrices for the three models trained on three different feature sets. Model 1 represents one of the current state of art approaches to identifying keratoplasties at-risk for a future rejection using qualitative scores defined by NIIOS. Model 2 represents a second current state of the art approach for identifying at-risk keratoplasties, and was trained on traditional morphometrics (ECD, CV, and number of cells). Finally Model 3 represents our approach and was trained on the top 10 quantitative imaging and cellular features. Model 3 (accuracy = 0.97 ± 0.04) outperformed Models 1 (accuracy = 0.78 ± 0.09) and 2 (accuracy = 0.93 ± 0.10).

Table 2. Quantitative metrics evaluating the performance of three trained models.

Feature Type	Accuracy	Sensitivity	Specificity	AUC
Model 1	0.78 ± 0.09	0.60 ± 0.15	0.95 ± 0.07	0.80 ± 0.06
Model 2	0.93 ± 0.10	0.87 ± 0.17	0.86 ± 0.17	0.86 ± 0.11
Model 3*	0.97 ± 0.04	0.91 ± 0.12	0.93 ± 0.06	0.92 ± 0.08

5. DISCUSSION

U-Net proves to be a sufficient learning system with regards to automatic segmentation of cell borders in clinical quality EC images post-keratoplasty. While EC automatic segmentation accuracy is very good, a couple small manual edits to each image can improve the accuracy even more. Following this step, we developed a Guided Manual Correction GUI software informing users of cells potentially segmented incorrectly, thus allowing users to manually edit the final automatic segmentation quickly. We think manual editing following automatic segmentation can be done in 3-5 minutes, which is much less in comparison to the 15-30 minutes now required for a full EC image manual segmentation.

Once the EC images are segmented, this provides an opportunity to measure and extract a large, robust collection of quantitative features on both a cellular and imaging level. We collect over 190 features describing the cellular intensity, textural, and shape characteristics and distributions, along with graph analytics from Voronoi tessellations, Delaunay triangulations, minimum spanning tree, etc. in addition to traditional morphometrics such as ECD and CV. To prove these features are more illustrative of a graft being at risk of an allograft rejection, we developed three machine learning algorithms trained on three different feature datasets: two state of the art feature datasets, and our proposed approach. Our proposed approach ultimately consists of ten features instead of 190, selected by mRMR feature selection as the most predictive between EC images from rejection and control grafts.

The most clinically relevant metric is the sensitivity of the model, or the ability to detect EC images of grafts that will eventually undergo a rejection. Missing a rejection early and allowing the endothelial damage to progress from the rejection process, can lead to graft failure and the need for a new transplant. Model 1, trained on qualitative scores evaluating cellular morphology, was only able to classify 38 of the 64 rejection images correctly for an average sensitivity of 0.60 ± 0.15 across 5-folds. Model 2, trained on traditional morphometrics classified 70 of 83 rejection EC images correctly for an average sensitivity of 0.87 ± 0.17 across 5-folds. Finally, Model 3, our proposed model trained on ten of the most predictive quantitative features correctly identified 74 of the 83 rejection EC images for a sensitivity of 0.91 ± 0.12 across 5-folds.

In summary, we developed a machine learning algorithm to extract a large, robust collection of quantitative features from challenging post-keratoplasty EC images to predict future graft rejection at least 1-3 months prior to clinical evidence of rejection. These findings offer the possibility of detection of at-risk corneas earlier before clinical signs (i.e. keratic precipitates, rejection line, edema) become apparent, thus offering the hope of lowering graft failure from rejection by altering anti-rejection therapies.

ACKNOWLEDGEMENTS

This project was supported by the National Eye Institute through Grant No. NIH R21 EY02949801 (DW and BAB) and NIH U10 EY012358 and U10 EY020798 (JHL and BAB). The grants were obtained via collaboration between Case Western Reserve University, University Hospitals Eye Institute, and Cornea Image Analysis Reading Center. The content of this report was solely the responsibility of the authors and does not necessarily represent the official views of the National Institutes of Health. There are no conflicts of interest. This work made use of the High-Performance Computing Resource in the Core Facility for Advanced Research Computing at Case Western Reserve University. The veracity guarantor, Chaitanya Kolluru, affirms to the best of his knowledge that all aspects of this paper are accurate. This research was conducted in space renovated using funds from an NIH construction grant (C06 RR12463) awarded to Case Western Reserve University.

REFERENCES

[1] Waring, G. O., Bourne, W. M., Edelhauser, H. F. and Kenyon, K. R., "The corneal endothelium. Normal and pathologic structure and function," Ophthalmology **89**(6), 531–590 (1982).

[2] Edelhauser, H. F., "The resiliency of the corneal endothelium to refractive and intraocular surgery," Cornea **19**(3), 263–273 (2000).

[3] Eye Bank Association of America, "Statistical Report," https://restoresight.org/what-we-do/publications/statistical-report/ (2019)

[4] Monnereau, C., Bruinsma, M., Ham, L., Baydoun, L., Oellerich, S. and Melles, G. R. J., "Endothelial Cell Changes as an Indicator for Upcoming Allograft Rejection Following Descemet Membrane Endothelial Keratoplasty," American Journal of Ophthalmology **158**(3), 485–495 (2014).
[5] Piorkowski, A., Nurzynska, K., Gronkowska-Serafin, J., Selig, B., Boldak, C. and Reska, D., "Influence of applied corneal endothelium image segmentation techniques on the clinical parameters," Computerized Medical Imaging and Graphics **55**, 13–27 (2017).
[6] Anna Fabijańska., "Segmentation of corneal endothelium images using a U-Net-based convolutional neural network," Artificial Intelligence in Medicine **88**, 1–13 (2018).
[7] Scarpa, F. and Ruggeri, A., "Automated morphometric description of human corneal endothelium from in-vivo specular and confocal microscopy," 2016 38th Annual International Conference of the IEEE Engineering in Medicine and Biology Society (EMBC), 1296–1299 (2016).
[8] Benetz, B. A., Lass, J. H., Sayegh, R., Mannis, M. J. and Holland, E. J., "Specular Microscopy," [Cornea: Fundamentals, Diagnosis, Management], Elsevier, 160–179 (2016).
[9] Benetz, B. A., Lass, J. H., Gal, R. L., Sugar, A., Menegay, H., Dontchev, M., Kollman, C., Beck, R. W., Mannis, M. J., Holland, E. J., Gorovoy, M., Hannush, S. B., Bokosky, J. E., Caudill, J. W. and Group, for the C. D. S. I., "Endothelial Morphometric Measures to Predict Endothelial Graft Failure After Penetrating Keratoplasty," JAMA Ophthalmol **131**(5), 601–608 (2013).
[10] Lass, J. H., Sugar, A., Benetz, B. A., Beck, R. W., Dontchev, M., Gal, R. L., Kollman, C., Gross, R., Heck, E., Holland, E. J., Mannis, M. J., Raber, I., Stark, W. and Stulting, R. D., "Endothelial Cell Density to Predict Endothelial Graft Failure After Penetrating Keratoplasty," Arch Ophthalmol **128**(1), 63–69 (2010).
[11] Sugar, A., Gal, R. L., Kollman, C., Raghinaru, D., Dontchev, M., Croasdale, C. R., Feder, R. S., Holland, E. J., Lass, J. H., Macy, J. I., Mannis, M. J., Smith, P. W., Soukiasian, S. H. and Beck, R. W., "Factors Predictive of Corneal Graft Survival in the Cornea Donor Study," JAMA Ophthalmol **133**(3), 246–254 (2015).
[12] Lass, J. H., Benetz, B. A., Patel, S. V., Szczotka-Flynn, L. B., O'Brien, R., Ayala, A. R., Maguire, M. G., Daoud, Y. J., Greiner, M. A., Hannush, S. B., Lee, W. B., Mauger, T. F., Menegay, H. J., Mifflin, M. D., Raizman, M. B., Rose-Nussbaumer, J., Schultze, R. L., Schmidt, G. A., Sugar, A., et al., "Donor, Recipient, and Operative Factors Associated With Increased Endothelial Cell Loss in the Cornea Preservation Time Study," JAMA Ophthalmology **137**(2), 185–193 (2019).
[13] O'Brien, R. C., Ishwaran, H., Szczotka-Flynn, L. B., Lass, J. H., and Cornea Preservation Time Study (CPTS) Group., "Random Survival Forests Analysis of Intraoperative Complications as Predictors of Descemet Stripping Automated Endothelial Keratoplasty Graft Failure in the Cornea Preservation Time Study," JAMA Ophthalmology doi:10.10001/jamaophthalmol.2020.5743 (2020).
[14] Cornea Donor Study Investigator Group, Lass, J. H., Gal, R. L., Dontchev, M., Beck, R. W., Kollman, C., Dunn, S. P., Heck, E., Holland, E. J., Mannis, M. J., Montoya, M. M., Schultze, R. L., Stulting, R. D., Sugar, A., Sugar, J., Tennant, B. and Verdier, D. D., "Donor age and corneal endothelial cell loss 5 years after successful corneal transplantation. Specular microscopy ancillary study results," Ophthalmology **115**(4), 627-632 (2008).
[15] Lass, J. H., Benetz, B. A., Gal, R. L., Kollman, C., Raghinaru, D., Dontchev, M., Mannis, M. J., Holland, E. J., Chow, C., McCoy, K., Price, F. W., Sugar, A., Verdier, D. D. and Beck, R. W., "Donor age and factors related to endothelial cell loss ten years after penetrating keratoplasty: Specular Microscopy Ancillary Study," Ophthalmology **120**(12), 2428-2435 (2013).
[16] Patel, S. V., Lass, J. H., Benetz, B. A., Szczotka-Flynn, L. B., Cohen, N. J., Ayala, A. R., Maguire, M. G., Drury, D. C., Dunn, S. P., Jeng, B. H., Jones, M. F., Menegay, H. J., Oliva, M. S., Rosenwasser, G. O. D., Seedor, J. A., Terry, M. A., Verdier, D. D., and Cornea Preservation Time Study Group., "Postoperative Endothelial Cell Density Is Associated with Late Endothelial Graft Failure after Descemet Stripping Automated Endothelial Keratoplasty," Ophthalmology **126**(8), 1076–1083 (2019).
[17] Lass, J. H., Benetz, B. A., Verdier, D. D., Szczotka-Flynn, L. B., Ayala, A. R., Liang, W., Aldave, A. J., Dunn, S. P., McCall, T., Mian, S. I., Navarro, L. C., Patel, S. V., Pramanik, S., Rosenwasser, G. O., Ross, K. W., Terry, M. A., Kollman, C., Gal, R. L., Beck, R. W., et al., "Corneal Endothelial Cell Loss 3 Years After Successful Descemet Stripping Automated Endothelial Keratoplasty in the Cornea Preservation Time Study: A Randomized Clinical Trial," JAMA Ophthalmology **135**(12), 1394–1400 (2017).
[18] Stulting, R. D., Lass, J. H., Terry, M. A., Benetz, B. A., Cohen, N. J., Ayala, A. R., Maguire, M. G., Croasdale, C., Daoud, Y. J., Dunn, S. P., Goins, K. M., Gupta, P. C., Macsai, M. S., Mian, S. I., Pramanik, S., Rose-Nussbaumer, J., Song, J. C., Stark, W. J., Sugar, A., et al., "Factors Associated With Graft Rejection in the Cornea Preservation Time Study," American Journal of Ophthalmology **196**, 197–207 (2018).

[19] Ronneberger, O., Fischer, P. and Brox, T., "U-Net: Convolutional Networks for Biomedical Image Segmentation," International Conference on Medical image computing and computer-assisted intervention **Springer, Cham** (2015).
[20] Naomi Joseph, Chaitanya Kolluru, Beth A. M. Benetz, Harry J. Menegay, Jonathan H. Lass, and David L. Wilson., "Quantitative and qualitative evaluation of deep learning automatic segmentations of corneal endothelial cell images of reduced image quality obtained following cornea transplant," Journal of Medical Imaging **7**(1), 1–13 (2020).